Noname manuscript No.
(will be inserted by the editor)

Evolution of nanostructures of anatase TiO_2 thin films grown on (001)$LaAlO_3$

Regina Ciancio · Andrea Vittadini · Annabella Selloni · Riccardo Arpaia · Carmela Aruta · Fabio Miletto Granozio · Umberto Scotti di Uccio · Giorgio Rossi · and Elvio Carlino

Received: date / Accepted: date

Abstract Combining reflection high energy electron diffraction, high resolution transmission electron microscopy and high angle annular dark field scanning transmission electron microscopy we unveil the existence of a peculiar transition from a three-dimensional to a two-dimensional growth mode in anatase $TiO_2/LaAlO_3$ heterostructures. Such a growth dynamics is accompanied by Al interdiffusion from substrate to the growing film up to a critical thickness of 20 nm. With the extra support of *ab initio* calculations, we show that the crossover between the two growth modes corresponds to the formation of two distinct regions characterized by (103)- and (101)-oriented crystallographic shear superstructures, occurring in the upmost film region and in proximity of the film/substrate interface, respectively.

Keywords Thin film structure and morphology · High resolution transmission electron microscopy · Composition, segregation; defects and impurities · Density functional theory, local density approximation, gradient and other corrections

PACS 68.55.-a · 68.37.Og · 68.35.Dv · 71.15.Mb

R. Ciancio and E. Carlino
CNR-IOM TASC, Area Science Park Basovizza, Trieste, I - 34146, Italy
email: ciancio@iom.cnr.it

G. Rossi
CNR-IOM TASC and Department of Physics, University of Milano, Via Celoria 16, I-20100 Milano, Italy

A. Vittadini
CNR-ISTM and CR-INSTM Village, c/o Department of Chemical Sciences, University of Padua, Via Marzolo 1, I-35131 Padova, Italy

A. Selloni
Department of Chemistry, Princeton University, Princeton, NJ 08544, USA

R. Arpaia, C. Aruta, F. Miletto Granozio, U. Scotti di Uccio
CNR-SPIN and Dipartimento di Scienze Fisiche, Complesso Universitario di Monte S.Angelo, Via Cintia, I-80126 Napoli, Italy

1 Introduction

Transition metal oxides form a broad and diverse class of materials (Rao 1998; Henrich and Cox 1994) among which TiO_2 holds a prominent role for its unique physico-chemical properties and promising technological applications, ranging from photocatalysis and solar energy conversion to electrodes for regenerative fuel cells and memresistor switching memories.(Weinberger and Garber 1995; Chen and Yang 2002; Jellison at al. 1997; Chen et al. 2002; Szot at al. 2011) The most common TiO_2 crystalline phases are rutile and anatase. Both structures can be described in terms of a tetragonal lattice where the basic building block consists of chains of distorted TiO_6 octahedra resulting in significantly different unit cells and distinct physical and chemical behavior(Ganduglia-Pirovano et al. 2007). In particular, rutile is the most thermodynamically stable, well-defined, and commercially available crystal phase. However anatase is more attractive as a photocatalyst and is usually obtained as single crystals in the form of nanomaterials. Also due to the difficulty in obtaining macroscopic single crystals, extensive studies have made it possible to grow highly crystalline epitaxial anatase thin films via several methods (Chambers 2010; Chang aet al. 1991; Murakami at al. 2001; Yamamoto et al. 2001; Lotnyk et al. 2007; Weng et al. 2008; Wang et al. 2010) and on a wide variety of substrates, the choice of the latter being of primary importance to obtain highly textured thin films. Among all substrates used, $LaAlO_3$ (LAO) is an ideal candidate, because its small lattice mismatch with anatase (about 0.2%)(Murakami et al. 2001; Kennedy and Stampe 2003, Schlom et al. 2008) is a prerequisite to obtain anatase thin films of good crystalline quality with clean and sharp TiO_2/LAO heterointerfaces. To date, in spite of substantial advances in the heteroepitaxial growth of TiO_2, a detailed understanding of the functional properties of the binary material is still lacking, due to their strong dependence on the

presence and type of defects. A systematic investigation of defects requires a careful characterisation of microstructure and of local chemical properties both of the film and of the film/substrate interface. The interfacial microstructures of TiO_2/LAO have been previously investigated (Murakami et al. 2001; Weng et al. 2008; Wang et al. 2010); however, the understanding of the film growth modes and generation of defects is still far from complete. Moreover, the interest in LAO/TiO_2 interfaces is enhanced by the close structural analogy with the widely studied LAO and TiO_2-terminated $SrTiO_3$ interfaces which show an unexpected two dimensional electron gas (Ohtomo and Hwang 2004; Banerjee et al. 2012). In order to analyze the evolution of the nanostructure of TiO_2 anatase thin films deposited on (001) LAO substrates, we combine in this work in-situ reflection high energy electron diffraction (RHEED), cross-sectional high resolution transmission electron microscopy (HRTEM), high angle annular dark field (HAADF) scanning TEM (STEM) analyses and first principle Density Functional Theory (DFT) calculations. We found an unusual three-dimensional (3D) to two-dimensional (2D) growth mode transition in the film structure which resulted in the formation of two adjacent slabs characterized by two distinct Magnéli-like superstructures each having different crystallographic matching with the bare substrate. Finally, we propose a model for the peculiar growth mode of the overlayer and draw conclusions on the role of cation interdiffusion on film nucleation.

2 Experimental and calculation details

TiO_2 films were deposited by pulsed laser deposition on untreated (001)LAO substrates held at 700C in a 10^{-1} mbar oxygen atmosphere. A KrF excimer laser beam (248 nm, 25 ns duration full width half maximum) was focused on a stoichiometric target with a fluence of $2J \cdot cm^{-2}$. The growth process was monitored in situ by RHEED which allows to evaluate thin film surface morphology during the growth process (Rijnders et al. 1997; Braun 1999). Briefly, in the RHEED technique, an electron beam strikes the sample surface at a grazing incidence angle and is diffracted onto a fluorescent screen. In the case of a 2D structure, the corresponding reciprocal space lattice consists of lines normal to crystal surface (rods). Since the RHEED image results from the intersection between the reciprocal lattice rods and the Ewald sphere, a 2D surface yields a streaky-pattern onto the phosphorous screen. However, in case of 3D structures, diffraction arises from 3D material islands. Similarly to the case of diffraction in transmission electron microscopy, the electron beam travels within nano-meter grains/islands, therefore reproducing their reciprocal lattice onto the phosphorous screen (yielding the so-called 3D spotty pattern).

Conventional x-ray diffraction analysis was performed on the TiO_2/LAO films by a Philips X'Pert-XRD analytic diffractometer equipped with a four-circle cradle. A Cu K_α (λ= 1.5406 Å) source was used at 40 kV and 40 mA.

TEM/STEM experiments were performed using a TEM/STEM JEOL 2010 UHR field emission gun microscope operated at 200 kV with a measured spherical aberration coefficient Cs = 0.47 $\pm$ 0.01 mm. The microscope is equipped with an Oxford system for energy dispersive X-ray spectroscopy (EDS) studies. HAADF images were acquired using an illumination angle of 12 mrad and a collection angle $88 \leq 2\theta \leq 234$ mrad. Cross-sectional samples in the [010] zone axis suitable for TEM/STEM analyses have been obtained by a conventional polishing technique followed by dimpling and ion milling. The ion mill process was performed following a well-established protocol to avoid preferential sputtering at the substrate/film interface (Carlino 2008).

DFT calculations were performed by using the Perdew-Burke- Ernzerhof (Perdew et al. 1996) parametrization of the generalized gradient approximation (GGA), both without and with the inclusion of onsite Coulomb repulsion U on the Ti 3d states(Anisimov et al. 1991) For the latter, the computed (Cococcioni 2005) value U = 3.5 eV was employed. We adopted the plane-wave pseudopotential scheme as implemented in the QUANTUM ESPRESSO package(Giannozzi et al. 2009) with the computational setup extensively tested in Ref. (Lazzeri et al. 2001). For the GGA+U calculations, we used the GGA-optimized lattice constants but reoptimized the internal degrees of freedom. More details on the calculations are in Ref. (Ciancio et al. 2012a).

3 Experimental results

3.1 Growth and in-situ RHEED analysis

Since RHEED image is expected to qualitatively change with respect to either 3D or 2D surface morphology, any qualitative change in the diffraction pattern evolution reveals immediately changes in the surface morphology structure (e.g. either 3D or 2D) of the growing film.

RHEED images of a typical TiO_2/LAO film at different deposition stages are shown in Fig.1. Fig.1a shows that the bare LAO substrate has a pure 2D termination as well as a twin structure (i.e. spitting of the RHEED diffracted spots) characteristic of the native presence of macroscopic ferroelastic domains (Geddo Lehmann et al. 2007). Nevertheless, the TiO_2 film initially grows in the 3D mode without showing any twinning effect induced by the substrate (see RHEED pattern of Fig.1b). The RHEED pattern keeps the same aspect up to a thickness of about 20 nm, when it evolves into a 2D streaky pattern (Fig.1c). This form is kept until the end of the process. Basically, RHEED indicates that at this stage the surface doesn't change; this is also demonstrated by the absence of oscillations in the reflected RHEED intensity, probably indicating that the growth takes

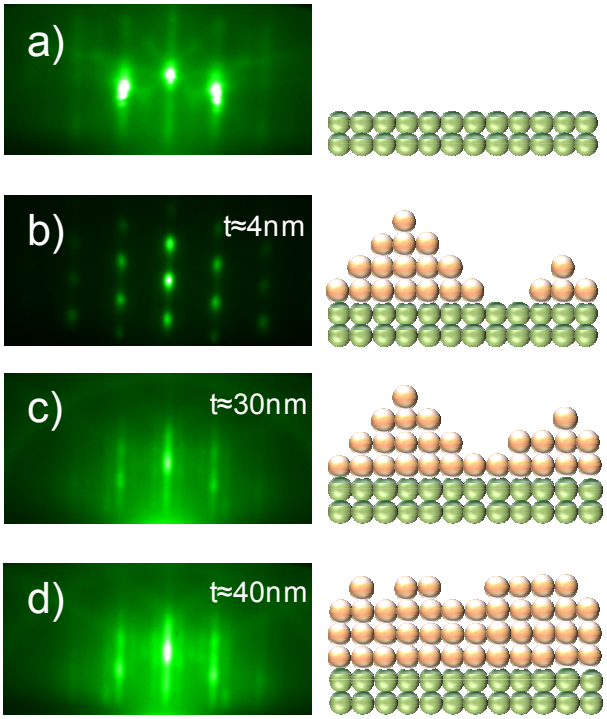

Fig. 1 Evolution of the RHEED pattern during the growth of TiO_2 thin film on $LaAlO_3$ substrate. On the left, RHEED pattern of the 2D terminated LAO substrate before the deposition (a), and at different stages of the TiO_2 growth, namely for film thickness of about 4 (b), 30 (c) and 40 nm (d), respectively. The splitting of the diffracted spots appearing in a) is characteristic of the native twin structure of LAO. On the right, a cartoon describing the surface morphology corresponding to the RHEED images.

place through crystal-steps flow. The high quality of the final surface is confirmed by the appearance of the well known 4×1 reconstruction, characteristic of (001) anatase. This is evident in Fig.1d, where the final pattern (at a thickness of 40 nm) is shown.

3.2 Structural analysis by X-ray diffraction

The crystallographic properties of the samples were explored by X-ray diffraction (XRD). Typical θ-2θ spectrum (main panel of Fig.2) only shows the (00l) peaks, indicating the preferential *c*-axis orientation of the film along the [001] substrate crystallographic direction. No impurity phases such as rutile TiO_2 or Ti_nO_{2n-1} phases were detected in the film, similarly to previous reports (Murakami et al. 2001, Weng et al. 2008). The out-of-plane parameter resulted to be 0.958 $\pm$ 0.001 nm, in a good agreement with the theoretical *c*-axis parameter of TiO_2 anatase. Specular reflectivity measurements were carried out to determine the thickness and the roughness of the TiO_2 film. Experimental reflectivity curve and simulation are shown in the inset of Fig.2. The simulation of the reflectivity curve was performed with the IMD code (Windt 1998) available in the XOP package (Sànchez del Rìo and Dejus 1998). The plot in the inset is the theoretical behavior of a film with a thickness of 40nm. The simulation yields a very low value of surface roughness (i.e. 1nm) which is compatible with the qualitative indications of the 2D nature of the RHEED pattern at the end of deposition.

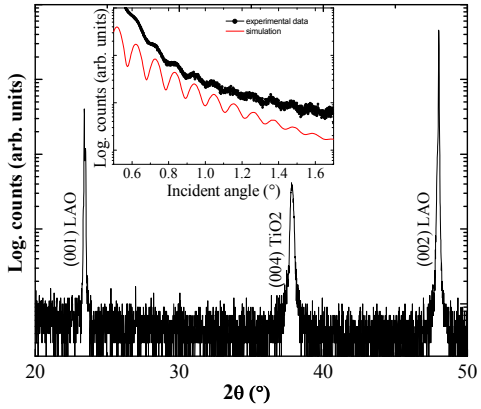

Fig. 2 θ-2θ spectrum of TiO_2 film grown on LAO substrate. Low-angle reflectivity measurements of the TiO_2 sample (black dots). Simulated reflectivity curve (red) is also reported on the graph.

3.3 Nanostructural characterisation

XRD reveal valuable information on the film chemical composition, indicating that a unique TiO_2 anatase phase is formed, but it provides quite limited insight into the microstructure. To get such information, we investigated several samples by TEM; in the following, data are shown for the same sample of Fig.2. A cross-sectional bright-field TEM image of a representative region of the TiO_2/LAO interface is shown in Fig.3a. The image was taken under multi-beam condition with the primary electron-beam along the [010] direction of the substrate. From this figure, one can see that the substrate surface is rather flat and entirely covered by the anatase TiO_2 film. The average measured thickness is 40 nm, in agreement with X-ray reflectivity. Interestingly, the bright field TEM image shows that the film is divided into two adjacent regions each about 20 nm thick (hereafter called I and II), each having different diffraction contrast.

Closer HRTEM inspection shows that the two slabs are characterized by a modulated structure typical of the existence of crystallographic shear (CS) planes, i.e. regular arrays of planar defects originated by oxygen vacancies throughout the film. The shear defects have different spacing and relative orientation with respect to the LAO substrate depending on the film region in which they are located. In particular, the upmost region of the film is populated by CS

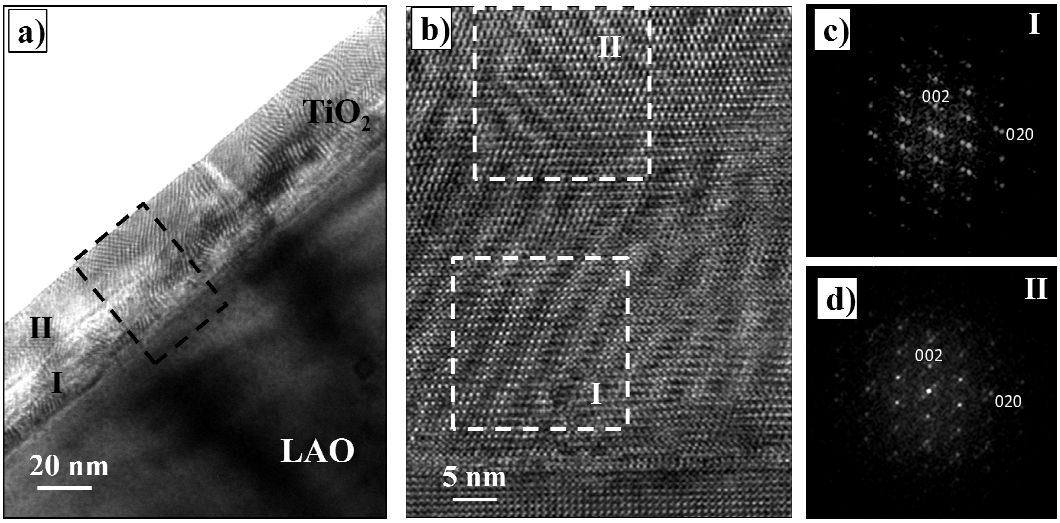

Fig. 3 (a)Bright field TEM image of the TiO_2/LAO film in the [010] zone axis showing the splitting of the film into adjacent regions (I and II) with different diffraction contrast. (b) HRTEM image in the [010] zone axis of the TiO_2/LAO interfacial region, showing the details of the two shear defects regions ; diffractrogram of the (c) I CS region and (d) II CS region

planes with a regular spacing of 1.3 nm which form a $\pm 38°$ angle with the in-plane LAO direction, whereas, the region close to the film/substrate interface, contains CS planes having 2.0 nm spacing and forming a $\pm 68°$ angle with [100]. The separation between the two CS regions coincides with the critical thickness, t$\sim$20 nm, at which the growth mode of the TiO_2 films changes. The multiple-peak trend of the diffractograms taken over the two CS regions displayed in Figs. 3(c) and 3(d) is characteristic fingerprint of the existence of two new superlattices defined by the two different families of CS planes in the film. Starting from the HRTEM results, we built two Ti_nO_{2n-1} (n=6) superstructures by removing either (101) or (103) layers of O atoms and optimized the structure by DFT calculations. In analogy with the Ti_nO_{2n-1} Magnéli phases of rutile, the microstructure of the two superstructures consists of alternate slabs of oxidized (TiO_2) and reduced (TiO) stoichiometry (see Fig.4), but extra Ti can be easily accommodated. In fact, DFT results indicate that phases of Ti_7O_{11} are particularly favored. This is validated by nearly-perfect correspondence between the HRTEM micrograph and simulated TEM images performed on the modeled structures(Ciancio et al. 2012b). In addition, computed formation energies of the two CS superstructures reveal that the (103) CS structure is largely favored with respect to the (101) CS one. Nevertheless, the (101) structure is stabilized in proximity of the interface due to the smaller lattice mismatch with substrate.

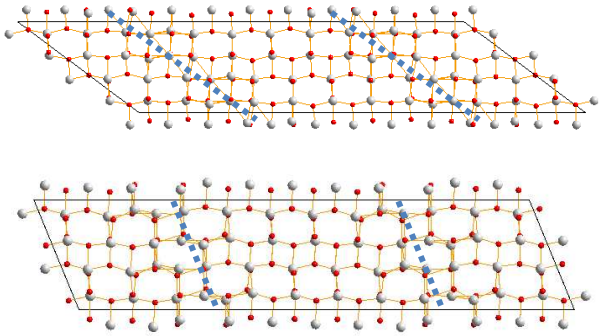

Fig. 4 Ball-and-stick models of the cells for the superstructures formed by (101) and (103) CS planes (highlighted by blue-dot lines)

By analysis using HAADF and EDS experiments, a second interesting property of the sample emerges. Figure 5 shows a typical HAADF-STEM image of the TiO_2/LAO interfacial region. Contrast variations are seen between the two slabs of the film. Since STEM dark field experiments produces images whose contrast is approximately proportional to the square of the average atomic number of the illuminated area (brighter contrast being associated with heavier elements), we can conclude that the region close to the substrate has a higher density compared to the outer region of the film. EDS analysis performed across the overall film/substrate interfacial region reveals indeed an Al diffusion from the substrate towards the film which substantially drops over about 15 nm with a residual slope until 20 nm. Cationic interdiffusion was observed also in TiO_2 anatase thin films deposited on $SrTiO_3$ substrates and was attributed to the reactivity of TiO_2 anatase with perovskite substrates(Ciancio et al. 2012a).

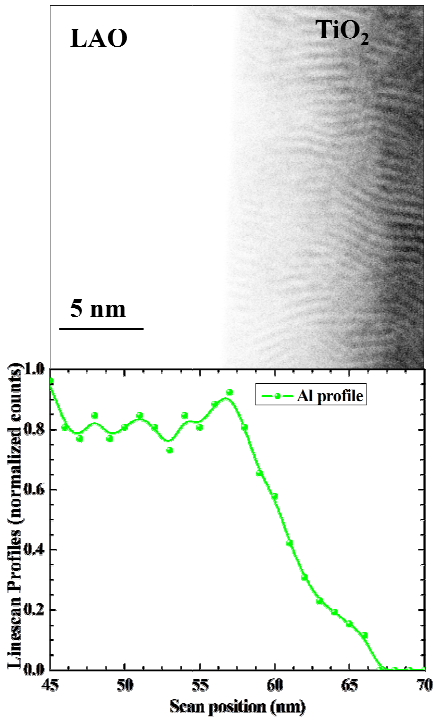

Fig. 5 (upper panel) HAADF/STEM image of the TiO_2/LAO interfacial region. (lower panel) EDS elemental profile of Al acquired on the area displayed in the image.

4 Discussion

The main achievement of this work is the evidence of the unusual crossover between 3D to 2D growth mode of anatase TiO_2 on LAO. Our data allow to relate this behaviour to the crossover from (101) to (103) shear planes. This indicates that the thermodynamically stable phase (i.e., phase II, hosting (103) CS) doesn't nucleate on the substrate, presumably due to a higher cost in term of elastic energy, connected to the worst match with the substrate. The reduction of strain is in fact accomplished in phase I by introducing (101) shear planes. It is reasonable to assume that each new such block may undergo incoherent growth, until coalescence, consistently with the 3D growth mode observed by RHEED at the initial stage. This idea also accounts for the formation of the slightly disordered pattern of shear planes of phase I. At the critical thickness, the constraint imposed by matching with the substrate is released and the thermodynamically stable phase II grows in the 2D mode, as demonstrated by RHEED. We note that the only relevant difference with phase I is microstructural, i.e., of geometrical character, since the stoichiometry remains the same. As reported above, in the early stage of the film growth (left panel in Fig.6), the Al diffusion from the LAO substrate to the growing film is observed, thus resulting in an alloyed Al_xTiO_z. In spite of the altered composition, the structural parameters of the overlayer are those of anatase-TiO_2 layer, which keeps the anatase-type coordination. Remarkably, diffusion is limited to 20 nm thickness, corresponding to the critical thickness at which phase II starts (Fig.6). The simplest explanation for this evidence is that Al migrates, at least partly, along the defective paths of the film, and that such paths are absent in Phase II. This circumstance may be relevant in determining the electronic properties of TiO_2 films, where Al may play the role of either point defect or of dopant, depending on its electronic state. We expect that both our work and further investigation of this issue may result in a considerable improvement of the heteroepitaxial growth of TiO_2 anatase thin films with targeted properties as well as for the understanding of fundamental properties in this material for device applications.

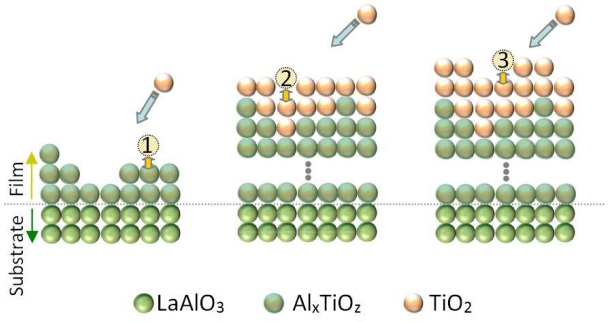

Fig. 6 Schematic diagram of the different stages of the growth process. On the left, TiO_2 ad-atoms impinging the bare LAO substrate, and resulting into an alloyed Al_xTiO_z compound; such a growth mode has been demonstrated by RHEED analysis to be 3D. At the center, at a critical thickness of about 20nm, Al diffusion ends, and impinging TiO_2 ad-atoms begins to grow as pure TiO_2; at this stage a transition from the alloyed Al_xTiO_z 3D final surface to a TiO_2 2D growth mode occurs. On the left, 2D growth mode lasts until the end of the deposition, as shown by the final RHEED image.

5 Conclusion

In conclusion, we determined an evolution along the growth direction of the nanostructure of anatase TiO_2 thin films grown on LAO substrates. Combining RHEED, XRD, HRTEM, HAADF and EDS analyses and the extra support of first principle calculations, we investigated the relation between growth mode and microstructure of the films. The growth is characterized by an unusual crossover from the 3D to the 2D mode at a critical thickness of about 20 nm. The structural analyses demonstrated that this corresponds to the formation of two slabs, both constituted by a Magnéli-like phase, differing one from each other for the orientation of the CS planes. Phase I, which contains (101) CS planes, shows a better matching with LAO; this allows its stabilization at the first stage. Phase II, which contains (103) CS planes, is thermodynamically favored and starts at the critical thickness

indicative of structural relaxation. EDS elemental profiles revealed the Al interdiffusion from the substrate towards the film up to the same critical thickness of 20 nm, suggesting that the onset of Phase II obstructs or annihilate the paths of diffusion.

Acknowledgements We are grateful to E. Cociancich for the assistance in the TEM specimen preparation. Valuable and fruitful scientific discussions with P. Orgiani are thankfully acknowledged. R.C.'s research activity has received funding from the European Community's Seventh Framework Programme 2007-2011 under grant agreement no. 212348 NFFA and Progetto strategico NFFA (fondi-MIUR). A.S. thanks the support of DoE-BES, Chemical Sciences, Geosciences and Biosciences Division, Contract No. DE-FG02-12ER16286.

References

1. Anisimov VI, Zaanen J, Andersen OK (1991)Band theory and Mott insulators: Hubbard U instead of Stoner I. Phys. Rev. B 44:943-954.DOI: 10.1103/PhysRevB.44.943
2. Banerjee N, Huijben M, Koster G, Rijnders G (2012) Direct patterning of functional interfaces in oxide heterostructures. Appl. Phys. Lett. 100:041601. DOI: 10.1063/1.3679379
3. Braun W (1999) Applied RHEED: Reflection High-Energy Electron Diffraction During Crystal Growth. Springer
4. Carlino E (2008) Quantification of chemical distribution of guest species in a host matrix by atomic resolution STEM Z-contrast. In: Salviati G, Sekiguchi T, Heun S, Gustafsson A (ed) Beam Injection Based Nanocharacterization of Advanced Materials. Research Signpost, Kerala, India, pp.237-242
5. Chambers SA (2010) Epitaxial growth and properties of doped transition metal and complex oxide films. Adv. Mater., 22:219-248. DOI: 10.1002/adma.200901867
6. Chang HLM, You H, Guo J, Lam DJ (1991) Epitaxial TiO_2 and VO_2 films prepared by MOCVD. Appl. Surf. Sci., 4849:12-18. DOI:10.1016/0169-4332(91)90301-Y
7. Chen JP, Yang RT (1993) Selective Catalytic Reduction of NO with NH_3 on $SO^{-2}{}_4/TiO_2$ Superacid Catalyst. J. Catal. 139:277-288. DOI: 10.1016/j.bbr.2011.03.031
8. Chen G, Bare SR, Mallouk TE (2002) Development of supported bifunctional electrocatalysts for unitized regenerative fuel cells. J. Electrochem. Soc. 149(8):A1092-A1099. DOI: 10.1149/1.1491237
9. Ciancio R, Carlino E, Aruta C, Maccariello D, Miletto Granozio F, Scotti di Uccio U (2012) Nanostructure of buried interface layers in TiO_2 anatase thin films grown on $LaAlO_3$ and $SrTiO_3$ substrates. Nanoscale, 4:91-94. DOI: 10.1039/c1nr11015b
10. Ciancio R, Carlino E, Rossi G, Aruta C, Scotti di Uccio U, Vittadini A, Selloni A (2012)Magnéli-like phases in epitaxial anatase TiO_2 thin films, Phys. Rev. B, 86:104110. DOI: 10.1103/PhysRevB.86.104110
11. Cococcioni M, deGironcoli S (2005) Linear response approach to the calculation of the effective interaction parameters in the LDA+U method. Phys. Rev. B 71:035105. DOI: 10.1103/PhysRevB.71.035105
12. Geddo Lehmann A, Sanna C, Lampis N, Congiu F, Concas G, Maritato L, Aruta C, Petrov AYu (2007) Effect of the substrate ferroelastic transition on epitaxial $La_{0.7}Sr_{0.3}MnO_3$ films grown on $LaAlO_3$. Eur. Phys. J. B 55:337345. DOI: 10.1140/epjb/e2007-00077-7
13. Giannozzi P, et al. (2009) QUANTUM ESPRESSO: a modular and open-source software project for quantum simulations of materials. J. Phys. Condens. Matter 21:395502. DOI:10.1088/0953-8984/21/39/395502
14. Henrich VE, Cox PA (1994) The Surface Science of Metal Oxides. Cambridge University Press, Cambridge.
15. Jellison GE, Modine FA Boatner LA (1997) Measurement of the optical functions of uniaxial materials by two-modulator generalized ellipsometry: rutile (TiO_2). Opt. Lett. 22:1808-1810. DOI: 10.1364/OL.22.001808
16. Kennedy RJ, Stampe, PA (2003) The influence of lattice mismatch and film thickness on the growth of TiO_2 on $LaAlO_3$ and $SrTiO_3$ substrates. J. Cryst. Growth 252:333-342. DOI: 10.1016/S0022-0248(02)02514-9
17. Lazzeri M, Vittadini A, Selloni A. (2001) Structure and energetics of stoichiometric TiO_2 anatase surfaces. Phys. Rev. B 63:155409. DOI: 10.1103/PhysRevB.63.155409
18. Lotnyk A, Senz S, Hasse D (2007) Epitaxial growth of TiO_2 thin films on $SrTiO_3$, $LaAlO_3$ and yttria-stabilized zirconia substrates by electron beam evaporation. Thin Solid Films, 515:3439-3447. DOI: 10.1016/j.tsf.2006.10.106
19. Murakami M, Matsumoto Y, Nakajima K, Makino T, Segawa Y, Chikyow T, Ahmet P, Kawasaki M, Koinuma H (2001) Anatase TiO_2 thin films grown on lattice-matched $LaAlO_3$ substrate by laser molecular-beam epitaxy. Appl. Phys. Lett., 78:2664-2666. DOI: 10.1063/1.1365412
20. Ohtomo A, Hwang HJ (2004) A high-mobility electron gas at the $LaAlO_3/SrTiO_3$ heterointerface. Nature 427:423-426. DOI:10.1038/nature02308
21. Perdew JP, Burke K, Ernzerhof M (1996) Generalized Gradient Approximation Made Simple. Phys. Rev. Lett. 77:3865-3868. DOI:10.1103/PhysRevLett.77.3865
22. Ganduglia-Pirovano MV, Hofmann A, Sauer J (2007) Oxygen vacancies in transition metal and rare earth oxides: Current state of understanding and remaining challenges. Surface Science Reports 62:219270. DOI:10.1016/j.surfrep.2007.03.002
23. Rijnders GJHM, Koster G, Blank DHA, Rogalla H (1997) In situ monitoring during pulsed laser deposition of complex oxides using reflection high energy electron diffraction under high oxygen pressure. Appl. Phys. Lett. 70:1888-1890. DOI:10.1063/1.118687
24. Rao CNR, Raveau B (1998) Transition Metal Oxides: Structure, Properties, and Synthesis of Ceramic Oxides, 2nd ed. Wiley-VCH, New York.
25. Sànchez del Rìo M, Dejus RJ, XOP: Recent developments (1998) SPIE Proc. 3448:340. DOI:10.1117/12.332522
26. Schlom DG, Chen LQ, Pan X, Schmehl A, Zurbuchen MA (2008) Thin Film Approach to Engineering Functionality into Oxides. J. Am. Ceram. Soc. 91:24292454. DOI: 10.1111/j.1551-2916.2008.02556.x
27. Szot K, Rogala M, Speier W, Klusek Z, Besmehn A, Waser R (2011)TiO_2-a prototypical memresistive material. Nanotechnology 22:254001. DOI:10.1088/0957-4484/22/25/254001
28. Yamamoto S, Sumita T, Sugiharuto T, Miyashita A, Naramoto H (2001) Preparation of epitaxial TiO_2 films by pulsed laser deposition technique. Thin Solid Films, 401:88-93.
29. Wang Z, Zeng W, Gu L, Saito M, Tsukimoto S, Ikuhara Y (2010) Atomic-scale structure and electronic property of the $LaAlO_3/TiO_2$ interface. J. Appl. Phys., 108:113701. DOI:10.1063/1.3516496
30. Weinberger B, Garber R (1995) Titanium dioxide photocatalysts produced by reactive magnetron sputtering. Appl. Phys. Lett. 66:2409-2411. DOI:10.1063/1.113956
31. Weng X, Fisher P, Skowronski M, Salvador PA, Maksimov O (2008) Structural characterization of TiO_2 films grown on $LaAlO_3$ and $SrTiO_3$ substrates using reactive molecular beam epitaxy. J. Cryst. Growth, 310:545-550. DOI:10.1016/j.jcrysgro.2007.10.084
32. Windt DL (1998) IMDSoftware for modeling the optical properties of multilayer films Comput. Phys. 12:360-370.